Models for numerical device simulations of crystalline silicon solar cells—a review

Pietro P. Altermatt

Abstract Current issues of numerical modeling of crystalline silicon solar cells are reviewed. Numerical modeling has been applied to Si solar cells since the early days of computer modeling and has recently become widely used in the photovoltaics (PV) industry. Simulations are used to analyze fabricated cells and to predict effects due to device changes. Hence, they may accelerate cell optimization and provide quantitative data e.g. of potentially possible improvements, which may form a base for the decision making on development strategies. However, to achieve sufficiently high prediction capabilities, several models had to be refined specifically to PV demands, such as the intrinsic carrier density, minority carrier mobility, recombination at passivated surfaces, and optical models. Currently, the most unresolved issue is the modeling of the emitter layer on textured surfaces, the hole minority carrier mobility, Auger recombination at low dopant densities and intermediate injection levels, and fine-tuned band parameters as a function of temperature. Also, it is recommended that the widely used software in the PV community, PC1D should be extended to Fermi-Dirac statistics.

Keywords Silicon solar cells · Numerical modeling · Device simulation · Raytracing

1 Overview on developments

Crystalline silicon solar cells have constituted the major part of industrially fabricated solar cells. Most of them are simple *p-n* junction diodes that cover the whole wafer area.

P.P. Altermatt (✉)
Department of Solar Energy, Institute for Solid-State Physics, Leibniz University of Hannover, 30167 Hannover, Germany
e-mail: altermatt@solar.uni-hannover.de

Their optimization is a complex task, because they are very well optically coupled to their surroundings, and their electrical performance depends strongly on the minimization of recombination and resistive losses. Despite of their simple diode structure, their performance usually cannot be described with analytical theories. Therefore, numerical solutions of the coupled semiconductor equations have been used for cell analysis since the early days of computer modeling. However, the PV industry has not relied on device modeling as much as the electronics industry. Changes to cell design evolved comparatively slowly, aided by a general understanding of device physics, by intuition, and empirical studies, but usually without the help of a thorough quantitative analysis by means of device modeling. Until the investment crisis in 2007/2008, the PV industry was more involved with scaling up than with improving device performance. It is a relatively young industry, with steeper declining experience curves [1] (price over accumulated production) than most of the electronics industry [2]. After 2008, however, the improvement of energy conversion efficiency became an important driver for competition among the companies. Since then, numerical device simulation has been in demand, for three main reasons:

– the highly-doped emitter has limited cell efficiency in most designs, and improvements are achieved by reducing its dopant density between the front metal fingers;
– two and three-dimensional patterning of dopant and contact regions at the rear surface bear a large potential for efficiency improvements; and
– improvements can be better achieved if the whole solar panel is included in design optimization.

The modeling software SENTUARUS [3], and to a smaller extend ATLAS [4] as well as MICROTEC [5] have become widely used in the PV industry. However, the physical models of these software packages have to be adjusted to the

specific demands of solar cells. This paper gives an overview over these specific demands.

2 Developments from a historical perspective

For most simulations of crystalline Si solar cells, it is sufficient to solve the semiconductor equations [6]

$$\nabla \cdot (\epsilon \nabla \psi) = -q(p - n + N_{don}^+ - N_{acc}^-), \tag{1a}$$

$$\frac{\partial n}{\partial t} = \frac{1}{q} \nabla \cdot \vec{J}_n + G - R, \tag{1b}$$

$$\frac{\partial p}{\partial t} = -\frac{1}{q} \nabla \cdot \vec{J}_p + G - R \tag{1c}$$

with the drift-diffusion approximation:

$$\vec{J}_n = -q\mu_n n \nabla \psi + q D_n \nabla n, \tag{2a}$$

$$\vec{J}_p = -q\mu_p p \nabla \psi - q D_p \nabla p. \tag{2b}$$

This coupled set of differential equations was used for cell analysis in the 60s soon after Gummel from Bell Labs [7] introduced an iterative procedure for its solution. An early example is the effort from Sandia National Laboratory in Albuquerque to model the radiation damage of Si cells for space applications [8]. With an improved code from Bell Labs [9], changes to cell design were suggested in the 70s for improving efficiency levels above 20% [10, 11].

In parallel to these efforts, a group at North Carolina State University developed refined simulation methods for solar cells [12–14]. An outstanding example are [15, 16], where the silicon part of the cell was calculated with a one-dimensional numerical solution of (1a)–(1c), and the losses in the metallization were accounted for by feeding the *I*-*V* curve of the one-dimensional simulation into a circuit of resistors. These simulations are probably the earliest account of *full-scale* modeling of solar cells.

At Purdue University, the software SCAP1D [17, 18] was developed and applied to solar cells in the early 80s, for example to analyze a current topic at the time: the limits to the open-circuit voltage [17, 19]. A particular success was the analysis of conductivity modulation in concentrator cells [20], which led to immediate device improvements. Device modeling also allowed to critically review measuring techniques, such as the Rose-Waver method in [21] which, as a result, was abandoned by the PV community. The SCAP1D software was soon extended to two dimensions and was called SCAP2D [22–25]. In two dimensions, it became possible to simulate a broad variety of different cell structures in the mid to late 80s, such as interdigitated back contact (IBC) cells, and etched multiple vertical junction (EMVJ)

cells. For an overview, see [19, 26]. Two-dimensional modeling made it possible to reproduce experimentally determined *I*-*V* curves of such cell structures and to derive dominating loss-mechanisms such as the break-down of charge-induced surface passivation at high illumination intensities [23]. Sometimes, device simulation was combined with process simulation, for example in the "Solar-Cell Efficiency Estimation Methodology and Analysis" (SEEMA) scheme at the Jet Propulsion Laboratory [27]. Simulations of two-dimensional cell structures became also possible with the software PISCES IIB [28] from Stanford University. With PISCES IIB, one of the earliest simulation of floating junctions were performed [29].

In the mid 80s, computer capacity improved to the point that (1a)–(1c) could be solved on a personal computer (PC). In the photovoltaics community, the one-dimensional semiconductor simulator PC1D was developed as a free-ware for a PC [30–32]. In contrast to most other semiconductor modeling software, it solves the equations not with the finite-difference but with a finite-element method [33]. This method is well suited for one dimensional semiconductors (but in 2D only under special circumstances [34], and in 3D it requires special basis functions [35]). For a comparison between the two approaches, see [36]. PC1D has strongly influenced the PV community and was continually improved [37–39]. In particular, PV specific models have been developed for PC1D, as will be explained in the next section. Later, the software ADEPT [40] was developed for simulating solar cells in two and three dimensions, but has been mainly applied to cells made of other materials than crystalline silicon. The software AFORSHET [41] is used mainly for heterostructures, e.g. crystalline wafers with amorphous layers.

The development of own code, such as the object-oriented software FLOODS [42–44], or a Monte Carlo simulation technique for transient analysis [45], became rare because the device simulator SIMUL became popular in the electronics industry in the early 90s, partly due to its improved numerical [46] and meshing methods [47, 48]. It was soon called DESSIS, and later called SENTAURUS DEVICE or TCAD, and became widely used in solar energy research institutes and recently in the PV industry. At the University of NSW in Sydney, SIMUL was used to analyze Si solar cells with record efficiency levels [49–51] and the computer modeling contributed significantly to the new world record efficiency in 1994 [52, 53]. This sparked renewed interest in device modeling. For example, there were nine papers on DESSIS simulations published at the 14th European PV Solar Energy Conference in Barcelona, Spain, in 1997. At the Institute of Solar Energy Systems (ISE) in Freiburg, Germany, DESSIS was applied in particular to emitters with a mesh-structure [54], thin cells on transparent substrates [55] and recently to rear-contacted cells [56, 57]

and combined with process simulation of gettering [58]. At the University of Constance, Germany, DESSIS was applied with a combination of sophisticated ray tracing mainly to mechanically-textured Si solar cells [59, 60]. Mainly metal-insulator-semiconductor (MIS) cells were investigated with DESSIS at the Institute for Solar Energy Research Hamelin (ISFH), Germany [61, 62], while later DESSIS has been used for industrial-type solar cells [63]. At IMEC in Belgium, the screen-printed cells were compared to buried contact cells by means of 2D DESSIS simulation [64]. Later, other research groups started to use DESSIS as well, see for example [65–70]. DESSIS made tree-dimensional modeling feasible, for an early example see [71], for the simulation of grain boundaries see [72, 73], for recent progress in the simulation of emitter-wrap-through (EWT) cells see [74]. Cells made of Si nanorods were simulated in [75, 76].

3 PV-specific demands on models

3.1 Demands on discretization

The numerical solution of (1a)–(1c) puts stringent conditions on the simulation mesh [47, 48, 77], which must be adapted to the geometry of the device. Most solar cells have an area of about 15×15 cm^2 and are about 180 µm thick, while their smallest features are below one micrometer. However, it is not necessary to simulate the entire cell because the structure of the semiconductor part is highly symmetric, so the simulation domain can be reduced to a geometrically irreducible *standard domain*. See Fig. 1 for an example. In many cell structures, this domain can even be two-dimensional, where its width is half the spacing between the front metal fingers, i.e. in the range of millimeters. In case that there are point-like contacts, the standard domain must be chosen three-dimensional and cannot be approximated with a two-dimensional finger geometry, for two main reasons. Firstly, the resistive losses are proportional to ρj^2, where ρ is the resistivity and j is the local current-density, which differs greatly between finger and point-like geometries. Secondly, the recombination losses depend sensitively on the minority carrier-density, given by the quasi-Fermi level $E_{F,min}$, and is connected to j via $j \propto \nabla E_{F,min}$. Hence, approximating a point-like contact with a two-dimensional finger geometry causes errors in both the resistive and the recombination losses.

Figure 2 shows an excerpt of a three-dimensional meshing geometry. The mesh must be fine where any input or output parameter varies strongly with distance, otherwise the discretization errors become significant. In solar cells, this is

1. near the front surface, where the blue part of the sunlight is absorbed within nanometers. A sufficient mesh resolution is given in Table 1;
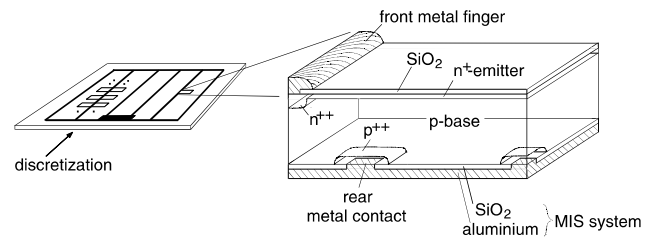

Fig. 1 Solar cells (*left*) are highly symmetric, so the geometrically irreducible domain of the device simulation is small and either three-dimensional (*right*) or even two-dimensional (not shown). The metallization pattern needs to be added with a circuit simulation
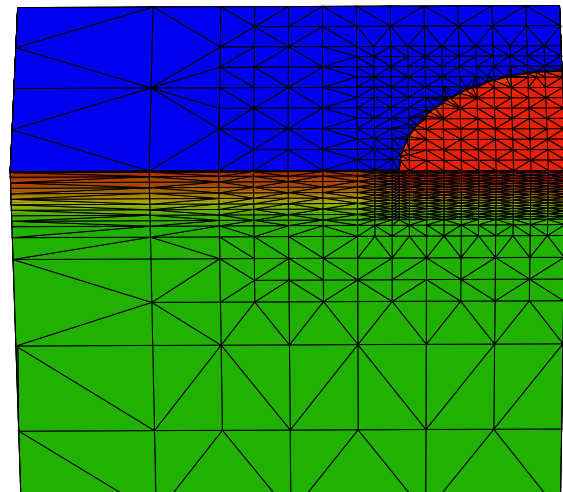

Fig. 2 The simulation mesh needs to be finer in regions where either an input or an output variable changes strongly over distance, like the current density near this rear circular contact. From SENTAURUS

Table 1 The mesh resolution (in units of µm) must be very fine in dependence of the depth (in µm) from the surface, because the blue part of the solar spectrum has a very short absorption length

Depth [µm]	Mesh resolution [µm]
0–0.002	0.001
0.002–0.02	0.02
0.02–0.1	0.04
0.1–4	1
4–8	2
8–16	4
16–32	8
32–64	16

2. the phosphorus-diffused front emitter, which has a depth of about 300 nm. It is usually well resolved due to 1;

3. near the metal contacts either at the front and, depending on cell design, also at the rear, where there is current-crowding.

In the base, the mesh may be chosen as coarse as 20 μm. Typical meshes therefore have less than 10 000 mesh points in 2D, and about 80 000 mesh points for simple 3D structures, a size which is easily manageable with present PC technology.

Figure 1 shows that the standard domain contains only a small part of the front metal grid. However, the cell can be thought of as being 'tiled' with standard domains [15, 16, 53], as indicated in Fig. 1. The 'tiling' must be discretized, because a typical cell would consist of a few thousand 3D standard domains. Finally, the chosen number of standard domains are connected in a circuit by ohmic resistances which represent the front metal fingers. For symmetry reasons only half of the front metal grid must be modeled.

The discretization errors induced with tiling depend on the boundary conditions of the standard domain. They are chosen such that current flows only through the metal contacts. Thus, the discretization error is small if, in real cells, the currents through silicon across these artificially introduced boundaries are negligible. This condition is usually fulfilled, because these boundaries are chosen considering the symmetries of the device. We only need to take care that the voltage drop along the front finger within each standard domain is negligible, and that the voltage difference is small between two neighboring fingers. Thus, it is possible to treat the standard domains in isolation, i.e. to first simulate one single standard domain, and afterwards feed its *I-V* curve multiple times into the circuit simulation.

Losses in the cell's perimeter region may be significant and may need to be included in full-scale modeling. It was shown in [78] that the perimeter region can be treated as a perturbation of the outermost standard domains, i.e. that the perimeter effect can be superimposed onto the behavior of a cell with ideal borders.

3.2 Models for band parameters

Solar cells demand specific simulation models that are different from most of the rest of the electronics industry, because the behavior of solar cells is strongly influenced by minority carriers. This can be understood as follows. In the dark and under forward bias V, electron current is injected into the n-type contact by means of an external current-voltage source. This current must flow through the second contact, but which is p-type, so any current through the diode requires recombination of electron-hole pairs to be maintained. The recombination rate is roughly proportional to the excess minority carrier density which, in turn, increases approximately exponentially with applied V (because the applied voltage lowers the barrier across the p-n junction by V). This is the primary reason why a diode has an exponential *I-V* curve shown in Fig. 3. The more recombination centers exists within the cell, the stronger is
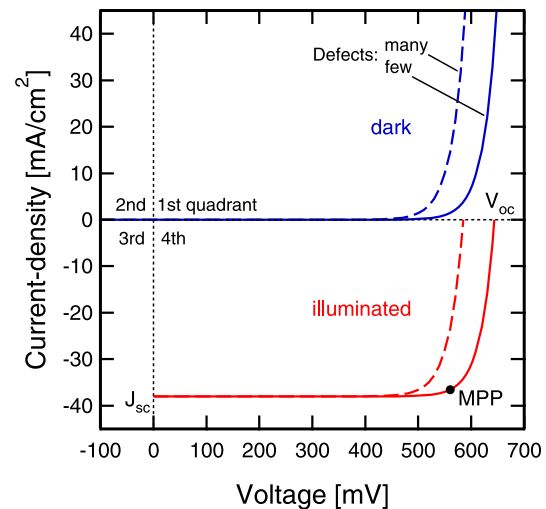

Fig. 3 The diode characteristics in the dark is shifted to the 4th quadrant under illumination, so the solar cell has the following *I-V* parameters: the short-circuit current density J_{sc}, the open-circuit voltage V_{oc}, while the output power $P = I \cdot V$ has its maximum at the maximum power point (MPP)

the exponential increase. Now consider the case were light is switched on. The current is generated *within* the device, as opposed to the dark where it is being injected *into* the device. Hence, the electron current flows *out* of the n-type contact, so the current-direction is reversed to negative values. This shifts the dark *I-V* curve down to the fourth quadrant as depicted in Fig. 3. Instead of applying a voltage with a current-voltage source, a photo-voltage is generated. The illuminated *I-V* curve has approximately the same shape as the dark *I-V* curve if one assumes that the quasi-Fermi levels per given external voltage are the same, regardless of the illuminated or dark case. Figure 3 shows that, if the cell contains many recombination centers, the *open-circuit voltage*, V_{oc}, is lower. This also lowers the power output $P = I \cdot V$, which is maximal somewhere on the *I-V* curve, called the *maximal power point* MPP. Hence, the performance of solar cells depends sensitively on the amount of recombination, and with this on the excess minority carrier density. This implies that the *pn*-product must be known very precisely, and with this the effective intrinsic carrier density

$$n_{i,eff}^2 = n_i^2 e^{\Delta E_g/(kT)}, \qquad (3)$$

where n_i is the intrinsic carrier density and ΔE_g is the band gap narrowing (BGN). BGN is important in solar cells, and so are the following three aspects:

– There is $\Delta E_g = \Delta E_c + \Delta E_v$, i.e. it is the sum of the band shifts of the conduction and valence bands, and the two shifts are not the same. However, experience shows that the usual procedure of $\Delta E_c = \Delta E_v = \Delta E_g/2$ induces no significant errors in the simulation of Si solar cells.
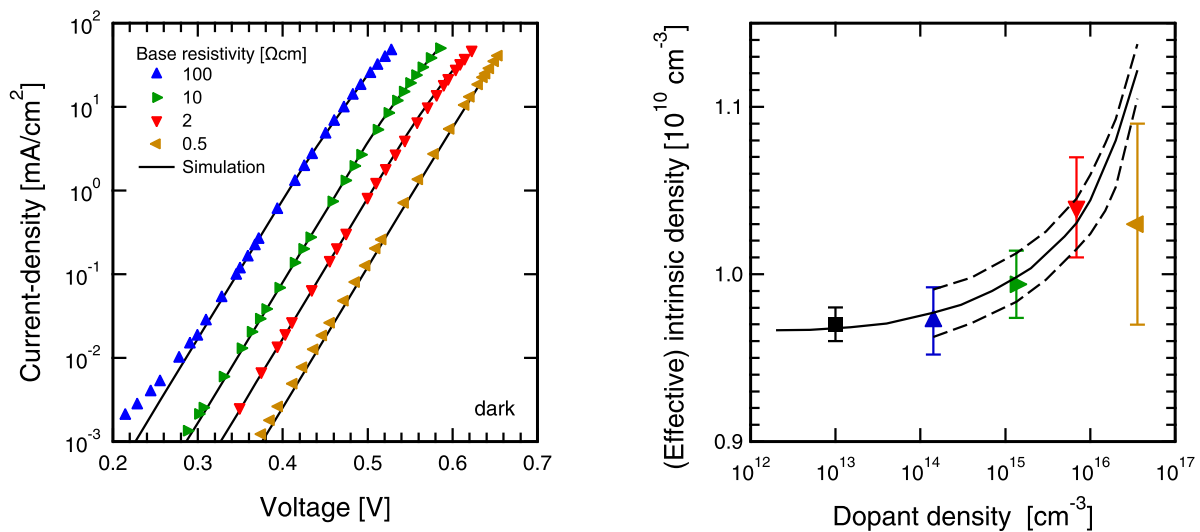
Fig. 4 *Left*: Dark *I-V* characteristics of Sproul and Green's samples [81]. *Right*: The n_i values extracted from the *I-V* characteristics with (4), as well as Misiakos and Tsamaki's n_i value [82] (*square symbol*), measured with admittance spectroscopy. The *solid line* is the reproduction of Sproul and Green's experiment by full-scale modeling, using Schenk's band gap narrowing model [84], the *dashed lines* show the uncertainties in the modeling due to the error bars in mobility measurements

– In many device simulators, BGN is parameterized as a function of dopant density N_{dop} in the low-injection regime where the excess carrier density $\Delta n \ll N_{dop}$. However, apart from carrier-dopant interactions, the carrier-carrier interaction is equally important, which makes ΔE_g a function of N_{don}, N_{acc}, n, and p. As long as a Si solar cell is operated at low-injection conditions, parameterizations of BGN as a function of N_{dop} are sufficiently precise. This is not the case in lowly-doped cells and cells under concentrated sunlight.

– Last but not least, BGN depends strongly on the chosen carrier statistics, as will be shown in more detail below.

In the following, the precise determination of n_i is taken as an example of how specific models were derived in the PV community. When people started simulating Si solar cells in the 70ies, they took the value of n_i from the electronics industry, which was commonly set to 1.45×10^{10} cm^{-3}. This choice caused a severe underestimation of V_{oc}. With a rather unnoticed exception [79], it took until 1990 to adjust n_i to lower values by means of experiments with high-efficiency Si solar cells that had a highly optimized emitter [80, 81]. The basic idea behind these experiments by Sproul and Green was as follows. The saturation current-density J_0 of a solar cell is the sum of the contributions from the emitter and from the base, i.e. $J_0 = J_{0,em} + J_{0,base}$. High-efficiency cells have a small $J_{0,em}$, so by deteriorating the rear surface, one arrived at $J_0 = J_{0,base}$, which is [80]

$$J_0 = qA \frac{n_i^2}{N_{dop}} \frac{\coth(W/L)}{L}. \tag{4}$$

This means that J_0 depends only on a small number of well-measurable parameters such as the dopant density in the base N_{dop}, the base width W, and the diffusion length L (A is the area of the cell). As n_i depends quadratically on J_0, n_i could be determined very precisely via J_0 measurements, i.e., via the dark *I-V* curves shown in Fig. 4(a). Various N_{dop} levels (or, equivalently, base resistivities) resulted in various n_i values depicted in Fig. 4(b), so the average was taken, which is $n_i = 1.00(3) \times 10^{10}$ cm^{-3} [81] (the digit in the parentheses represents the estimated one-standard-deviation uncertainty in the last digit of the previous value). However, this value was significantly higher than $9.7(1) \times 10^9$ cm^{-3} as determined with admittance measurements by Misiakos and Tsamakis [82] and is shown as square symbol in Fig. 4(b). Later, the experiment of 1990 was simulated with a full-scale numerical model [83]. The main result was that the measurements of both methods could be consistently explained with applying Schenk's quantum-mechanically derived BGN model [84], see the solid line in Fig. 4(b). It implies that BGN starts to have an effect at very low dopant densities, so Sproul and Green's experiment yielded $n_{i,eff}$ instead of n_i, and n_i turned out to be $n_i = 9.65(3) \times 10^9$ cm^{-3} [83], consistent with the value of Misiakos and Tsamakis [82].

The fact that Schenk's BGN model was successful had two further implications. Firstly, BGN has a significant influence on cell behavior down to lower N_{dop} values than was previously expected in the PV community. Earlier, when the high $n_i = 1.45 \times 10^{10}$ cm^{-3} was commonly used, BGN started to have an effect at $N_{dop} > 1 \times 10^{18}$ cm^{-3}, as shown in the data collection of del Alamo and Swanson [85] in
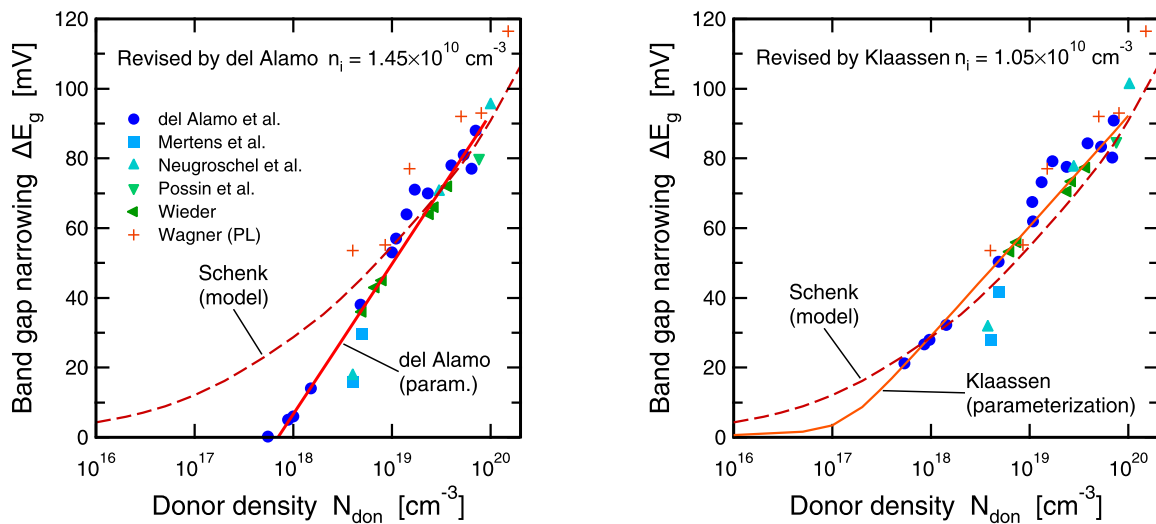
Fig. 5 A compilation of band gap narrowing measurements after a revision by del Alamo [85] (*left*) and Klaassen [86] (*right*), and a comparison to the quantum-mechanical model of Schenk [84]
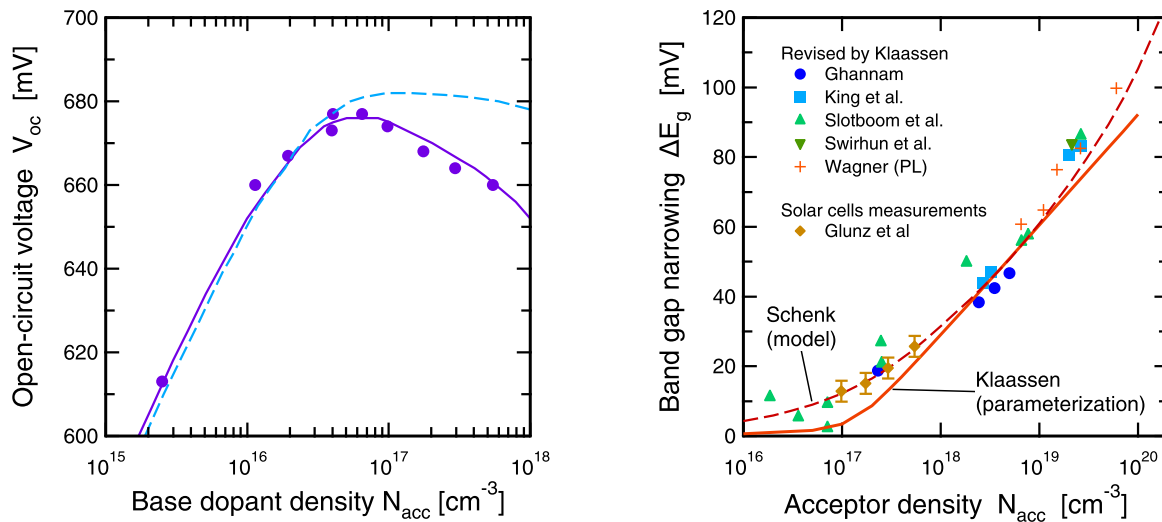

Fig. 6 *Left*: Measured open-circuit voltage V_{oc} of Si solar cells [87] with various base dopant density (*symbols*), compared to modeling using Schenk's band gap narrowing model [84] (*solid line*) or using a constant $n_i = 1.00 \times 10^{10}$ cm^{-3} (*dashed line*). *Right*: Band gap narrowing implied from V_{oc} via modeling (*diamonds with error bars*), compared to a revision of measurements by Klaassen [86] and Schenk's quantum-mechanical model [84]

Fig. 5(a). With a revision to lower n_i values, BGN became more significant at lower N_{dop}, as shown in the data collection of Klaassen et al. [86] in Fig. 5(b). In hind sight, an overestimation of n_i pulled the BGN values to lower values and forced BGN to disappear at low N_{dop}.

The second implication of Schenk's model [84] was that the cell's V_{oc} as a function of base doping had to be reassessed. Figure 6(a) shows experimentally determined V_{oc} values as a function of base doping [87]. The maximum near $N_{dop} = 6 \times 10^{16}$ cm^{-3} is well explained with Schenk's BGN model (solid line), while a constant $n_i = 1.00 \times 10^{10}$ cm^{-3} of Sproul and Green cannot describe the decline at higher

N_{dop} sufficiently well (dashed line), even if Klaassen's BGN model is used, which is shown as dash-dotted line in Fig. 5(b) . These experiments with solar cells confirmed Schenk's BGN model at low N_{dop} to a high level of precision, as indicated by the diamond symbols in Fig. 6(b). It is not surprising that solar cells are suitable for measuring BGN very precisely: from an electronics point of view, solar cells are large-area diodes with highly optimized and passivated emitters.

Adjusting n_i to the lower value of $9.65(3) \times 10^9$ cm^{-3} [83] necessitates an adjustment of the effective masses of
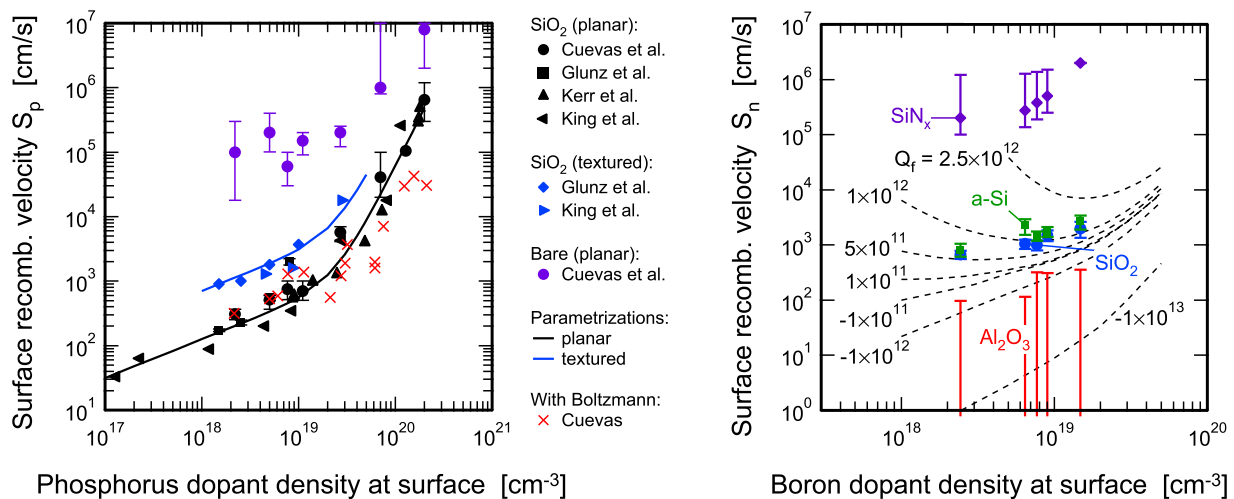
Fig. 7 *Left*: The surface recombination velocity parameter S_p at phosphorus-diffused surfaces passivated with SiO_2 or bare, extracted from J_0 measurements using Fermi-Dirac statistics or Boltzmann statistics (*crosses*), and a parameterization [99]. *Right*: The surface re-combination velocity parameter S_n at boron-diffused surfaces for various passivation layer materials, extracted from J_0 measurements using Fermi-Dirac statistics [100, 101], and the simulated influence of the fixed charge Q_f in the passivation layer (*dashed lines*)

electrons m_e^* and holes m_h^* via:

$$n_i^2 = N_v(m_h^*) N_c(m_e^*) e^{-E_g/(kT)}. \tag{5}$$

So far, the values of Green [88] have been most commonly used, which are given between T of 4.2 to 500 K and yield $n_i = 1.07 \times 10^{10}$ cm^{-3} at 300 K. As solar cells usually operate between $-40°C$ and $80°C$ in terrestrial applications, it does not matter whether E_g is adjusted to slightly larger values or whether m_h^* is lowered. The first option is convenient but not physically meaningful, because E_g is rather precisely known, see for example (23) of [89] (use this equation with $E_g(0)$ from [90] and Δ from [91]). The second option makes physically sense because m_h^* is least precisely known, but is rather intricate because there are two degenerate heavy-hole branches and a light split-off branch in the E-k relation. Setting up a set of band parameters that is consistent with the low n_i is definitely an area where more work is needed.

3.3 Impact from carrier statistics

After the band structure parameters, the applied carrier statistics have important consequences to modeling. Schenk's BGN model [84] is not an apparent BGN, so it needs to be used together with Fermi-Dirac statistics. It may surprise readers from other parts of electronics than photovoltaics that the PV community has used Boltzmann statistics for a long time, and sometimes does so even today. This has been so despite the fact that, in most industrially fabricated cells and also in many cells under development, device regions with $N_{dop} \gtrsim 2 \times 10^{19}$ cm^{-3} contribute significantly to the total recombination losses. In this doping

regime, Boltzmann statistics overestimates the pn product (as the Pauli blocking is absent), and this has been compensated for by introducing an *apparent* BGN that is lower than the actual one in (3) [92]. Although it has been shown in the early days of electronics that apparent BGN values cannot consistently compensate for the usage of Boltzmann statistics [93], apparent BGN models were very common. In the following, it is outlined why simulations using apparent values may point to inefficient cell optimization strategies.

As solar cells are large-area diodes, it is important to reduce recombination losses at the surfaces by surface passivation. The quality of surfaces is usually quantified by the surface recombination velocity S in units of cm/s:

$$R_{surf} = \Delta n_s S, \tag{6}$$

where R_{surf} is the recombination rate at the surface and Δn_s is the excess carrier density at the surface (note that at charged surfaces, $\Delta n \neq \Delta p$, so Δn_s is taken in the quasi-neutral region near the surface, and S is then replaced by the effective S_{eff}). The main issue is that, at highly-doped surfaces, S cannot be directly and precisely measured. A useful way has been to determine $J_{0,em}$ by means of excess carrier lifetime measurements with the method of Kane and Swanson [94] and using refined photoconductance decay methods of Sinton and Cuevas [95–98]. These J_0 measurements are then reproduced with modeling. We will see below that all modeling parameters, relevant to $J_{0,em}$, are known in the bulk of the emitter to a rather high precision, so S is adjusted as the sole free parameter in the modeling of the $J_{0,em}$ measurements. A collection of resulting S values for various passivation layers [99–101] is plotted in Fig. 7. Note

that S increases with increasing N_{dop} if Fermi-Dirac statistics is used, but decreases again toward high N_{dop} if Boltzmann statistics is applied (see the crosses), and even negative S values would be necessary to simulate regions with $N_{\text{dop}} > 4 \times 10^{20}$ cm^{-3}, i.e. many types of industrial emitters. This implies that, if Boltzmann statistics is used, $J_{0,\text{em}}$ may be well reproducible, but the relative contributions of surface and bulk recombination to the total emitter losses are distorted, and misleading conclusions to optimization strategies of emitters may be drawn. In addition, one and the same S cannot describe emitters with the same peak dopant density but different junction depth. Also note that the Auger recombination rate (discussed in Sect. 3.6) depends on the minority carrier density as well and may be overestimated with Boltzmann statistics.

By the way, J_0 depends quadratically on n_i [94], but various n_i values are used in the extraction of J_0 from lifetime measurements. In the simulations, the measured J_0 values have to be scaled to $n_i = 9.65 \times 10^9$ cm^{-3}. It would be useful if the PV community adopted the custom to mention the applied n_i when publishing J_0 measurements, and the exact temperature during the measurement.

There are two main reasons why Boltzmann statistics have been used in solar cell simulations. The first is that the software PC1D has only Boltzmann statistics implemented and is widely used in the PV community. Secondly, the electrons interact among each other in Fermi-Dirac statistics due to the Pauli blocking, so the Einstein relation $D = \mu kT/q$ is not valid and an additional term in the electron transport equation

$$-nkT\nabla\left(\ln\left(\frac{n}{N_c}e^{(E_c - E_{F,n})/(kT)}\right)\right) \qquad (7)$$

and a similar term in the hole transport equation is necessary. Therefore, no analytic solutions of simple problems are possible any more. With today's available semiconductor modeling software, no additional convergence problems are experienced when applying Fermi-Dirac statistics, because the Fermi-Dirac integral can be approximated [102] to avoid computational overload, and experience shows that the term (7) does not pose any problems (it is necessary so no current flows in the equilibrium condition $n = N_c F_{(1/2)}$). It is recommended here to use Fermi-Dirac statistics together with the S and BGN values that were extracted using this statistics, and also to implement Fermi-Dirac statistics and (7) into PC1D, which is a freeware available on sourceforge.net.

3.4 Transport equations at high dopant or injection densities

The usage of Fermi-Dirac statistics does not solve all the problems experienced in heavy doping. Unresolved issues involve BGN and the mobility of free carriers. It has been well known that heavy doping causes band tails at both band edges [103, 104]. Most of the tail states host immobile carriers [105, 106], while the BGN values relate to the *pn*-product, which means to *free* carriers. Hence, band tailing affects BGN only if a significant fraction of free carriers are related to tail states. At what N_{dop} this is the case in *c*-Si, and to which extent, is rather unclear, because the tail models—successfully applied to *a*-Si and microcrystalline Si—cannot be applied in a straight forward manner to the relatively low degree of disorder in highly-doped *c*-Si.

Some uncertainties exist in the mobility of free carriers at high doping densities. In the emitters of most industrially fabricated cells, interstitial phosphorus atoms and sometimes even precipitation of phosphorus exist [107], which may lower the carrier mobility but is not included in mobility parameterizations. Fortunately, the peak dopant densities of industrial emitters are presently reduced to improve cell efficiency, so the uncertainties in the carrier mobility becomes rather insignificant.

Uncertainties of the hole minority carrier mobility at lower dopant densities still prevail, see Fig. 8 for an overview of experimental values compared to the Klaassen's unified mobility model [108, 109], which distinguishes between majority and minority carriers and is therefore widely used in the PV community. The mobility differs between minority and majority carriers because the screening and scattering is different. Recently, heavily compensated material such as upgraded metallurgical grade (UMG) material has become available, and the evaluation of the carrier mobility is in progress [110–113]. To be precise, mobility would need to be parameterized as a tensor where the relative current-directions of electrons and holes are taken into account, especially in highly-injected solar cells [114–116]. A more detailed evaluation of minority carrier mobility and refined mobility parameterizations would be beneficial for modeling Si solar cells.

The influence of excitons on the operation of Si solar cells was discussed in the literature. Initial investigations indicated a significant influence [116–120], but they trace back to the oversimplified mass action constant [121], which only considers bound excitons and neglects the scattering states, and significantly overestimates the exciton density near $N_{\text{dop}} = 10^{18}$ cm^{-3}. According to the numerical calculations performed in [122] with the Planck-Larkin partition function, a physically reasonable upper limit for the population of excitons at $T = 300$ K is well below a few percent of the total electron and hole densities. Hence, no significant improvements with three-carrier transport equations (for electrons, holes and excitons) [117] are expected. By the way, both bound and free exciton states have been taken into account in Schenk's BGN model and in the consideration of Fig. 4. Schenk's BGN model is derived with a
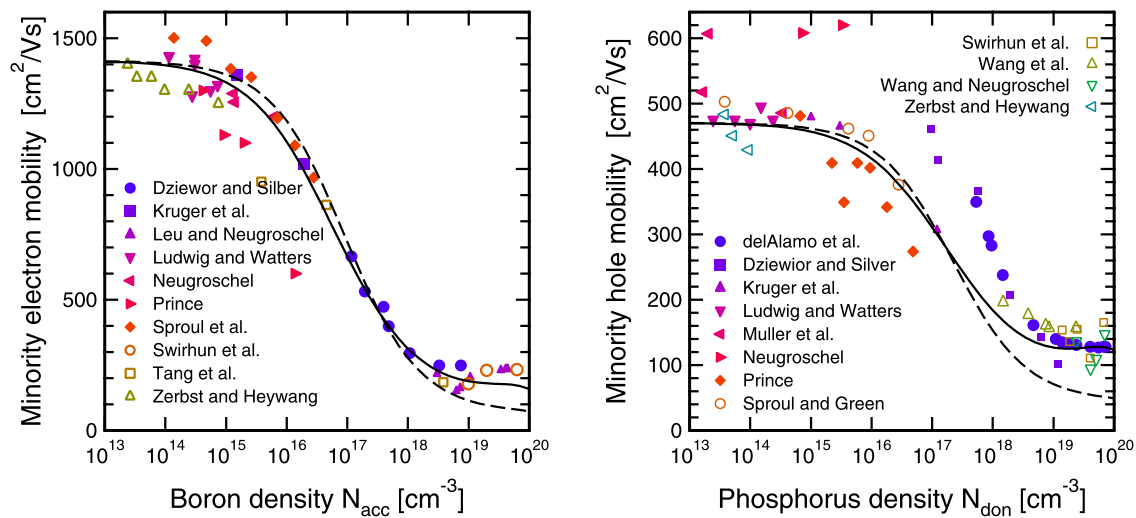
Fig. 8 The *symbols* show the measured minority electron mobility $\mu_{e,min}$ (*left*) and minority hole mobility $\mu_{h,min}$ (*right*). Klaassen's parametrization [108, 109] of the minority mobility is shown as *solid lines*, and of the majority mobility as *dashed lines*

finite-temperature full random-phase approximation (RPA), hence it is a rigid shift model. It was extended to the full RPA contribution on the basis of the statically screened ladder approximation (SSLA) in [83, 122], showing no significant effects at $N_{dop} < 2 \times 10^{19}$ cm^{-3}.

3.5 SRH recombination

In most parts of Si solar cells, recombination via states in the forbidden band gap can be well described [123] by means of the well-known Shockley-Read-Hall (SRH) theory [124, 125]:

$$R_{SRH} = \frac{pn - n_{i,eff}^2}{\tau_p(n + n_1) + \tau_n(p + p_1)}. \quad (8)$$

For the meaning of the symbols, see [124, 125]. Exceptions are recombination via amphoteric defects (e.g. dangling bonds) under certain circumstances [126, 127] and local shunt regions [128, 129], where defects have such a high density that they cannot be treated in isolation.

In the early days of Si solar cell simulation, the SRH lifetime $\tau_{SRH} = \Delta n/R_{SRH}$ was experimentally observed and simulated as doping-dependent and parameterized with the Scharfetter relation, also called Kendall formula [10, 130] (in some papers, this relation was used for the effective lifetime, which also comprises the Auger lifetime). In modern float-zone (Fz) silicon materials, such a dependence of the SRH lifetime is not observed any more up to the Auger limit of about $N_{dop} \approx 5 \times 10^{16}$ cm^{-3} [131, 132]. Hence, the lifetime parameters τ_n and τ_p can be assumed as doping-independent in (8). Note that τ_{SRH} is still injection dependent, e.g. a function of Δn because, say in *p*-type material, there is $\tau_{SRH} = \tau_n$ in low-injection condition because the

electrons limit the SRH rate, while there is $\tau_{SRH} = \tau_n + \tau_p$ in high-injection condition, where both carrier types exist in similar densities. In the early days of Si solar cell modeling, the injection condition during lifetime measurements was not always considered important but affected the results. When taking lifetime measurements as input parameters, one may need to consider that they may be differential values of injection-dependent lifetimes [133–136].

The injection-dependence of SRH lifetime may significantly influence the behavior of solar cells [63, 137, 138]. For example, a rather lowly-doped base may go from low towards high-injection condition when going from MPP towards open-circuit condition. Or Δn is considerably lower under non-favorable illumination conditions, and so may be the lifetime and, in turn, cell efficiency. In Czochralski-grown (Cz) boron-doped Si material, τ_{SRH} is strongly injection-dependent due to the boron-oxygen complex with the SRH parameters [139–141]:

$$\tau_n \,[\mu s] = 4.02024 \times 10^{45}[B_s]^{-0.824}[O_i]^{-1.748}m,$$
$$\tau_p \,[\mu s] = 10\tau_n, \quad (9)$$
$$E_d \,[eV] = E_c - 0.41,$$

where $[B_s]$ is the substitutional boron density, $[O_i]$ the interstitial oxygen density, and m is a processing-dependent parameter between 2 and 4. This means that $\tau_n + \tau_p$ is about 11 times higher than τ_n. This defect state is formed under illumination, so cell efficiency may degrade after initial illumination [142] if recombination via this defect level contributes significantly to the cell's total recombination losses.

In aluminum-doped silicon, the aluminum-oxygen complex reduces the SRH lifetime [143, 144]. This increases J_0 of Al-alloyed back surface fields (BSF) [63, 145, 146] and

Table 2 The mesh resolution (in units of μm) must be very fine in dependence of the depth (in μm) from surfaces that are passivated with a dielectric layer having a fixed charge

Depth [μm]	Mesh resolution [μm]
0–0.03	0.01
0.03–0.1	0.05
0.1–0.5	0.2

must be taken into consideration in modeling, especially of industrial-type Si solar cells.

Most surfaces of present-day Si cells are passivated with a dielectric layer with a fixed charge Q_f, so the electrostatic conditions need to be included in the model and a well-resolved simulation mesh must be generated in the surface regions, as listed in Table 2. The defect density at such interfaces is usually sufficiently small and Q_f is sufficiently large that the trapped charge in these states (due to their occupation statistics) can be neglected, so SRH recombination describes the situation well:

$$R_{\text{surf}} = \frac{p_s n_s - n_{\text{i,eff}}^2}{(1/S_p)(n_s + n_1) + (1/S_n)(p_s + p_1)}. \qquad (10)$$

An exception may be passivation layers made of amorphous silicon (a-Si), where the trapped charge should be included in the model [147]. As the defect states usually have a broader distribution at surfaces than in the bulk, the question arises whether the recombination rate can be sufficiently precisely modeled assuming a singe defect state. Again, this is indeed the case with the exception of a-Si passivation at certain injection-conditions. Figure 9 shows a collection of S_{eff} data as symbols. Note that the SRH parameters cannot be uniquely determined from Fig. 9, that means various sets of S_n, S_p and Q_f can result in the same S_{eff} behavior. The reason for this is the mathematical structure of the SRH equation. To extract unique SRH parameters of a defect, lifetime spectroscopy needs to be applied, where τ_{SRH} is measured in dependence of both injection level and temperature [140, 143, 148]. Additional effects arise if there are multiple defect types that can be treated independently from each other with SRH theory [149], and if the bulk near the surface has a low lifetime [150, 151]. At grain boundaries, two models of SRH recombination that are consistent with an extensive series of measurements are given in [72, 73]. For a general overview on lifetime, see [152].

3.6 Intrinsic recombination

For modeling Si solar cells sufficiently precisely, models for radiative and Auger recombination had to be refined.

At high dopant densities, Auger recombination dominates SRH recombination, and the coefficients for Auger
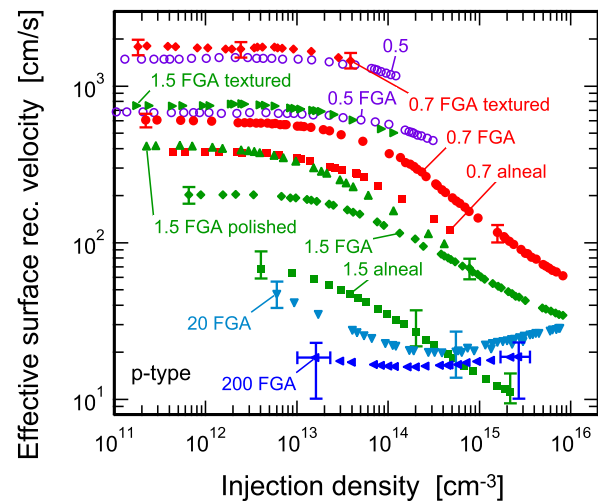
Fig. 9 Measured effective surface recombination velocity S_{eff} in dependence of injection density in p-type Si wafers (some polished or textured, most of them shiny etched) passivated with SiO_2, some using a forming gas anneal (FGA) or an Al anneal (alneal). Absolute (not differential [133–136]) values from ISFH

recombination C_n and C_p were already determined in the 70ies [132], e.g. by Dziewior and Schmid [153]. However, the recombination rate in solar cells may depend also sensitively on Auger recombination at dopant densities below approximately 10^{18} cm^{-3}, e.g. in the base region, and the extrapolation of C_n and C_p to these low dopant regime underestimates the Auger recombination rate. The reason for this is screening. Electrons and holes generally attract each other with their Coulomb force. At high carrier densities where e.g. Dziewior and Schmid determined C_n and C_p, electron-hole pairs are so efficiently screened by the large amount of other electrons and holes that electrons and holes in general can be treated as an ideal gas. This is why Dziewior and Schmid's C_n and C_p coefficients are independent of dopant density. However, towards lower carrier densities than about 10^{18} cm^{-3}, electron-hole pairs are less efficiently screened because there are far fewer electrons and holes, so they attract each other. Electron-hole pairs can only recombine if their wave functions overlap in space. The Coulomb attraction between the electron and the hole increases this overlap, and so does C_n and C_p towards lower carrier densities [154, 155]. To take account of this Coulomb enhancement, one keeps C_n and C_p as measured at high dopant densities but multiplies them with the enhancement factors g_{eeh} and g_{ehh} in the Auger rate equation:

$$R_{\text{Au}} = (g_{\text{eeh}} C_n n + g_{\text{ehh}} C_p p)(pn - n_{\text{i,eff}}^2). \qquad (11)$$

This means that g_{eeh} and g_{ehh} are unity at high N_{dop}, while they are larger than unity at lower N_{dop}, see Fig. 10. To which extent they are larger than unity is not sufficiently precisely known and a few different parameterizations exist
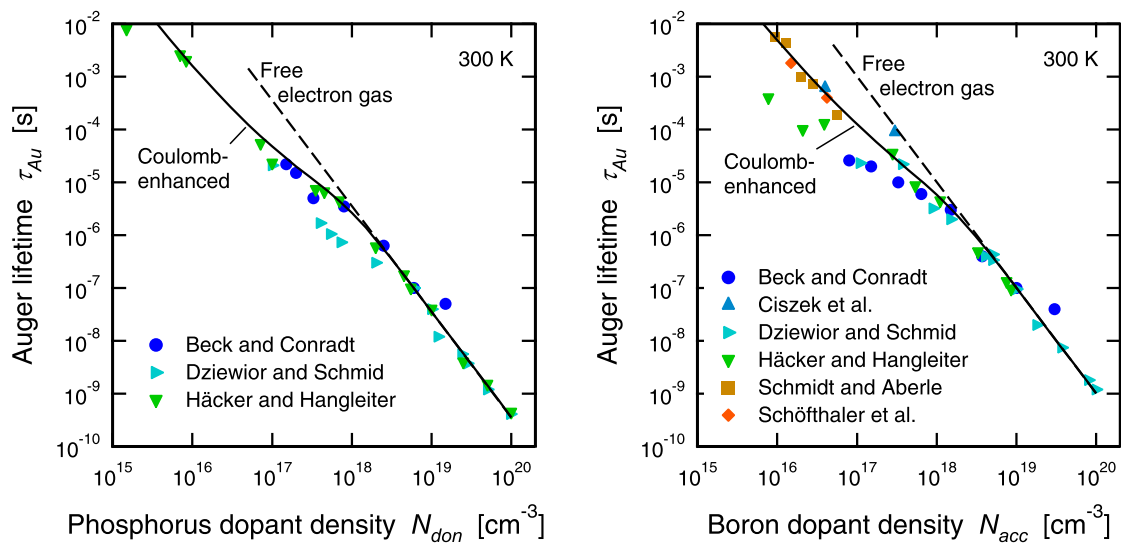
Fig. 10 Measured Auger lifetimes (*symbols*) compared to the free electron gas theory (*dashed line*), and the parametrization of (11) and Table 3 of Coulomb enhancement

Table 3 A consistent set of models and parameters for the simulation of Si solar cells.

Device simulation	
Equations numerically solved	Semiconductor equations [6]
Temperature	300 K
Free carrier statistics	Fermi-Dirac
Intrinsic carrier density	$n_i = 9.65 \times 10^9$ cm^{-3} [83]
Band gap narrowing model	Schenk [84]
Free carrier mobility	Klaassen's unified mobility model [108, 109]
Radiative recombination (12)	$B = 4.73 \times 10^{-15}$ cm^3/s [164]
Auger recombination (11)	Dziewior and Schmid [153]
Its temperature dependence [132]:	$C_{(n,p)} = (A + B(T/T_0) + C(T/T_0)^2)(1 + He^{-(n,p)/N_0})$
	$A = 2.8 \times 10^{-31}, 7.91 \times 10^{-32}$ cm^6/s
	$B = 0, -1.239 \times 10^{-32}$ cm^6/s
	$C = 0, 3.231 \times 10^{-32}$ cm^6/s
	$H = 8, 8$
	$N_0 = 2.5 \times 10^{17}, 2.5 \times 10^{17}$ cm^{-3}
SRH bulk recombination	boron-doped Cz Si, see (9)
SRH surface recombination	Phosphorus-diffused surfaces [99]
	Boron-diffused surfaces [100, 101]

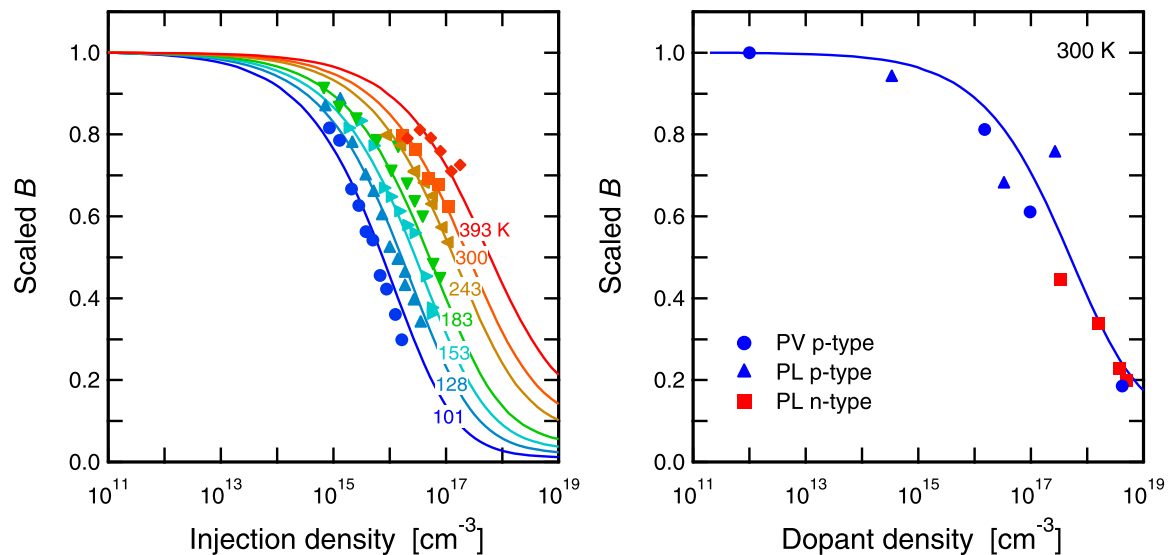| Optical simulation	
Solar spectrum	am0 from Gueymard [181]
	am1.5g and am1.5d calculated from [181] with SMARTS [182]
Optical dispersion relations:	
	Si from Green [183]
	Al from Shiles [184]
	Other metals from Palik [185]
	Many antireflection coatings are lab-specific

Fig. 11 Measured coefficient for radiative recombination B in (12) scaled to unity at low densities, as a function of injection density (*left*) or dopant density (*right*) obtained with photovoltaic (PV) or photo- luminescence (PL) methods. The *lines* are the parametrization from [163] (see footnote 1)

[156–159] that span the whole injection range. Uncertainties exists especially at low dopant densities and in the transition between low and high-injection. See [160] for an overview. Therefore, the Auger parametrization in Table 3 is rather un- certain and needs to be improved. Unfortunately, the widely used parametrization by Kerr and Cuevas [159] cannot be used in numerical device modeling because it is a polyno- mial expression with a too crude derivative, so the Auger recombination rate becomes exorbitant in space charge lay- ers.

The fact that the amount of screening influences g_{eeh} and g_{ehh} explains why at high-injection conditions, the ambipolar Auger Coefficient $C_a = g_{eeh}C_n + g_{ehh}C_p = 1.66 \times 10^{-30}$ cm^6/s [156] is larger than $C_n + C_p = 3.79 \times 10^{-31}$ cm^6/s [153], which has been an important issue in the simulation of Si concentrator cells [25, 156, 161].

The radiative recombination rate is influenced by the amount of screening as well. Figure 11 shows its depen- dence on injection and dopant density at various tempera- tures [162], for an empirical expression see [163].[1]

Apart from its dopant and injection dependence, the co- efficient of radiative recombination B in

$$R_{rad} = g_{eh}B(pn - n_{i,eff}^2) \qquad (12)$$

was under dispute [164] because its extraction from mea- surements depended strongly on the used n_i value, which underwent various revisions as discussed in Sect. 3.2. The value consistent with the revised $n_i = 9.65 \times 10^9$ cm^{-3} [83]

is $B = 4.73 \times 10^{-15}$ cm^3/s. It was derived from measure- ments of the Si photoluminescence spectrum. According to Kirchhoff's law [165], the emissivity is directly related to the absorptivity, so a favorable side-effect of the experiment was the determination of the wavelength-dependent absorp- tion coefficient for band-to-band transitions α_{bb} [166, 167], shown in Fig. 12. Note that with Kirchhoff's law, values as low as $\alpha_{bb} = 10^{-22}$ cm^{-1} could be measured, which corre- sponds to an absorption length of $1/\alpha_{bb} = 10\,000$ lightyears. It is unthinkable to determine such low values with transmis- sion spectroscopy.

3.7 Photogeneration

Figure 12 leads us to the last PV-specific issue, the calcu- lation of the carrier generation profile G in (1a)–(1c). For the calculation of G, the PV community has a long tra- dition of geometrical ray tracing models including TEX- TURE [168], the model in PC1D [32], SUNRAYS [169], RAYN [170], SONNE [171], RAYSIM [172], and recently DAIDALOS [173]. These models are all fully three-dimen- sional but most of them choose a simulation domain that contains only a single pyramid at the front surface. In con- trast, the device simulation usually has a standard domain that extends to half of the finger spacing and—as shown in Fig. 1—assumes a planar emitter. To incorporate the result of the raytracer into the device simulation, the photogener- ation rate $G(x, y, z)$ is projected onto a line that is oriented perpendicular to the solar cell (for example along the vertical y axis in Fig. 1). This one-dimensional profile $G(y)$ is then mapped laterally onto the entire standard domain of the de- vice simulation. When doing so, it is convenient to neglect

---

[1]In (4) of [163], b_1 should be replaced with $2b_1$, and b_2 with $2b_2$.
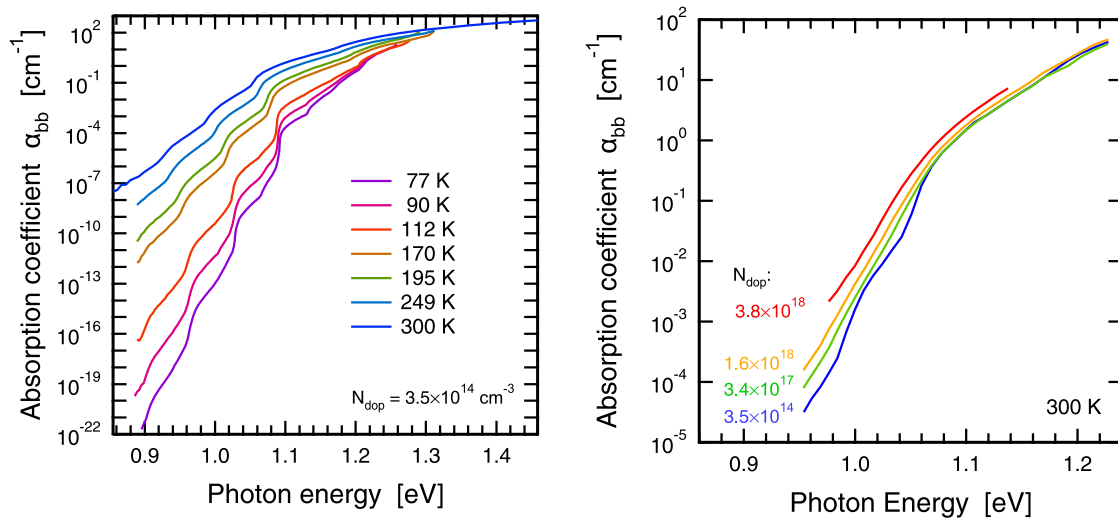
Fig. 12 Coefficient for band-to-band absorption of lowly-doped (*left*) and moderately-doped (*right*) crystalline silicon, deduced from photoluminescence measurements [162, 164]

the shading due to the front metal fingers, and instead to scale the current-values of the I-V curves inserted into the circuit simulation by the amount of shading, because then the device simulations do not need to be repeated if the finger width is varied in the circuit simulations. This procedure is suitable only if the amount of recombination at the front metal contacts is small compared to the cell's total recombination losses. It usually does not have any effect that the device parts directly beneath the front metal are illuminated with this procedure, because the front metal fingers are usually much narrower than the diffusion length of the device. It is important to note that the amount of shading is considerably lower than the front metal coverage [174–176], even if the cell is not encapsulated in a module. The reason for this is that much of the light reflected from the fingers is either directed downwards toward the silicon or is totally internally reflected at the air/glass interface.

The main errors in the optical generation of the device simulation usually arise because the mapped $G(y)$ is used: it has a maximum near the base of the pyramid while, in reality, $G(x, y, z)$ has its maximum at the surface [171]. See Fig. 13. To shift the maximum of $G(y)$ close to the surface, one chooses a pyramid size in the optical model that is far smaller than the average pyramid size in the experiment (e.g. 100 nm). If the emitter has a small collection efficiency near the surface (a dead layer), the short-circuit current J_{sc} depends rather sensitively on the pyramid size in the optical simulation. Fortunately, the PV industry is currently improving their emitters, so these issues become obsolete. A more sophisticated approach is to divide the volume close to the emitter surface in layers parallel to the surface [170]. Carriers generated within the layers of equal distance to the surface are counted for the respective 1D depth coordinate,
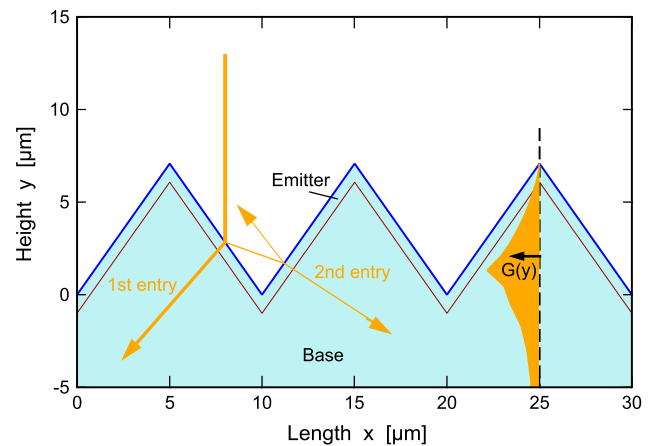

Fig. 13 The photogeneration rate $G(x, y, z)$ of a pyramidally textured front surface has its maximum at the surface. However, if it is projected onto the vertical y axis, $G(y)$, is has its maximum near the base of the pyramid. If $G(y)$ is mapped laterally onto the entire planar standard domain of the device simulation, most of the electron-hole pairs are generated below the emitter, unless the pyramid is chosen to be significantly smaller than in reality

since they have approximately equal probability of reaching the *pn*-junction.

There are two common sources of errors in the optical model. Firstly, the short wavelengths of sunlight are comparable to the size of the smallest features in the front texture, so the reflectivity depends on the roughness of the surface. This effect cannot be included in the optical model because it is based on geometrical rather than diffractive optics. In contrast to thin-film solar cells, full-scale optical simulations via solution of Maxwell's equations for realistic geometries have not been commonly applied to wafer-based *c*-Si cells, because the simulation domain is too large for

present computer capacities. Solving Maxwell's equations only in a locally restricted domain was done in [177] for investigating the impact of the roughness of the Al metallization on the overall rear reflectance. However, none of the above-mentioned ray tracers was able to accept the far-field solution of the local domain as an input, so no ray tracing was performed. Secondly, some ray tracers do not include free carrier absorption, which reduces the light intensity but does not create electron-hole pairs. In the absence of free carrier absorption, the cell's total reflectivity at long wavelength is overestimated. Models for free-carrier absorption are described in [178, 179]. Finally, the Fresnel equations for calculating the reflection and transmission at optical interfaces assume that the first medium is not absorptive, and the question arises of how to calculate the reflection at the cell's rear surface. Usually, sunrays that penetrate the whole cell and reach the rear surface have a wavelength where the extinction (or absorption) coefficient of silicon is rather small. In this case, the Fresnel equations induce only marginal errors [180].

4 Conclusions

The Table 3 lists a choice of electrical and optical models and parameters for the simulation of crystalline silicon solar cells. In this paper, it was described how this set of models and parameters has been developed over years with the help of various institutions, and a high level of consistency has been reached. The most approximative aspects are the Auger recombination rate at low dopant densities and intermediate injection levels, the hole minority carrier mobility, and the band parameters as a function of temperature should be fine-tuned to the $n_i = 9.65 \times 10^9$ cm^{-3}.

References

1. van Sark, W.G.J.H.M., Alsema, E.A., Junginger, H.M., de Moor, H.H.C., Schaeffer, G.J.: Prog. Photovolt. **16**, 441 (2008)
2. Hossain, T.M.: J. Manag. Mark. Res. **6**, 1 (2011)
3. Sentaurus. Synopsys, Mountain View, CA
4. Atlas. Silvaco, Santa Clara, CA
5. MicroTec. Siborg Systems Inc, Waterloo, Canada
6. van Roosbroeck, W.: Bell Syst. Tech. J. **29**, 560 (1950)
7. Gummel, H.: IEEE Trans. Electron Devices **27**, 1520 (1964)
8. Gwyn, C.W., Scharfetter, D.L., Wirth, J.L.: IEEE Trans. Nucl. Sci. **14**, 153 (1967)
9. Scharfetter, D., Gummel, H.: IEEE Trans. Electron Devices **16**, 64 (1969)
10. Fossum, J.: Solid-State Electron. **19**, 269 (1976)
11. Fossum, J.G.: IEEE Trans. Electron Devices **24**, 322 (1977)
12. Graham, E.D., Hauser, J.R.: Solid-State Electron. **15**, 303 (1972)
13. Dunbar, P.M., Hauser, J.R.: In: Proceedings of the 12th IEEE Photovoltaic Specialists Conference. IEEE Press, New York (1976)
14. Hauser, J.R., Dunbar, P.M.: IEEE Trans. Electron Devices **24**, 305 (1977)
15. Fang, C.R., Hauser, J.R.: In: Proceedings of the 13th IEEE Photovoltaic Specialists Conference, pp. 1306–1311. IEEE Press, New York (1978)
16. Fang, C.R., Hauser, J.R.: In: Proceedings of the 13th IEEE Photovoltaic Specialists Conference, pp. 1318–1326. IEEE Press, New York (1978)
17. Lundstrom, M.S.: Ph.D. thesis, School of Electrical Engineering, Purdue University, West Lafayette, IN (1980)
18. Girardini, K., Jacobsen, S.: Tech. Rep. N87-22301, NASA, Scientific and Technical Information (STI) (1986)
19. Schwartz, R.J., Turner, G.B.: In: Proceedings of the 19th IEEE Photovoltaic Specialists Conference, pp. 19–24. IEEE Press, New York (1987)
20. Schwartz, R.J., Lundstrom, M.S., Nasby, R.: IEEE Trans. Electron Devices **28**, 264 (1981)
21. Banghart, E.K., Schwartz, R.J., Gray, J.L.: In: Proceedings of the 18th IEEE Photovoltaic Specialists Conference, pp. 825–830. IEEE Press, New York (1985)
22. Gray, J.: Ph.D. thesis, School of Electrical Engineering, Purdue University, West Lafayette, IN (1982)
23. Gray, J.L., Schwartz, R.J., Lundstrom, M.S., Nasby, R.D.: In: Proceedings of the 16th IEEE Photovoltaic Specialists Conference, pp. 437–441. IEEE Press, New York (1982)
24. Gray, J.L., Schwartz, R.J.: In: Proceedings of the 17th IEEE Photovoltaic Specialists Conference, pp. 1297–1302. IEEE Press, New York (1984)
25. Banghart, E., Gray, J., Schwarz, R.: In: Proceedings of the 20th IEEE Photovoltaic Specialists Conference, pp. 717–722. IEEE Press, New York (1988)
26. Gray, J.L., Schwartz, R.J.: In: Proceedings of the 18th IEEE Photovoltaic Specialists Conference, pp. 568–572. IEEE Press, New York (1985)
27. Mokashi, A.R., Daud, T., Kachare, A.H.: In: Proceedings of the 18th IEEE Photovoltaic Specialists Conference, pp. 573–577. IEEE Press, New York (1985)
28. Pinto, M.R., Rafferty, C.S., Yeager, H.R., Dutton, R.W.: Tech. rep., Stanford Electronics Laboratories, Stanford University (1985)
29. Ghannam, M., Demesmaeker, E., Nijs, J., Mertens, R., Van Overstraeten, R.: In: Proceedings of the 11th European Photovoltaic Solar Energy Conference, pp. 45–48. Harwood Academic Publishers, Chur (1992)
30. Rover, D.T., Basore, P.A., Thorson, G.M.: In: Proceedings of the 18th IEEE Photovoltaic Specialists Conference, pp. 703–709. IEEE Press, New York (1985)
31. Basore, P.A., Rover, D.T., Smith, A.W.: In: Proceedings of the 20th IEEE Photovoltaic Specialists Conference, pp. 389–396. IEEE Press, New York (1988)
32. Basore, P.A.: IEEE Trans. Electron Devices **37**, 337 (1990)
33. Thorson, G.M., Basore, P.A.: Comput. Mech. Publ. **2**, 6 (1991)
34. Buturla, E.M., Cottrell, P.E., Grossman, B.M., Salsburg, K.A.: IBM J. Res. Dev. **25**, 218 (1981)
35. Angermann, L., Wang, S.: Appl. Numer. Math. **46**, 19 (2003)
36. Engl, W.L., Dirks, H.K., Meinerzhagen, B.: Proc. IEEE **71**, 10 (1983)

37. Basore, P.A.: In: Proceedings of the 22nd IEEE Photovoltaic Specialists Conference, pp. 299–302. IEEE Press, New York (1991)

38. Basore, P.A., Clugston, D.A.: In: Proceedings of the 25th IEEE Photovoltaic Specialists Conference, pp. 377–381. IEEE Press, New York (1996)

39. Clugston, D.A., Basore, P.A.: In: Proceedings of the 26th IEEE Photovoltaic Specialists Conference, pp. 207–210. IEEE Press, New York (1997)

40. Gray, J.L.: In: Proceedings of the 22nd IEEE Photovoltaic Specialists Conference, pp. 436–438. IEEE Press, New York (1991)

41. Froitzheim, A., Stangl, R., Kriegel, M., Elstner, L., Fuhs, W.: In: Proceedings of the 3rd World Conference on Photovoltaic Energy Conversion, pp. 279–282. IEEE Press, New York (2003)

42. Liang, M., Law, M.L.: IEEE Trans. Comput.-Aided Des. Integr. Circuits Syst. **13**, 1235 (1994)

43. Fossum, J.G., Sarkar, D., Mathew, L., Rao, R., Jawarani, D., Law, M.E.: In: Proceedings of the 35th IEEE Photovoltaic Specialists Conference, pp. 792–797. IEEE Press, New York (2010)

44. Jimeno, J.C., Uriarte, S., Zamora, J.J., Icaran, C.: In: Proceedings of the 10th European Photovoltaic Solar Energy Conference, pp. 75–78. Kluwer Academic, Dordrecht (1991)

45. Bosso, S., Shamsi, T.A., Krebs, K.H., Manfredotti, C.: In: Proceedings of the 18th IEEE Photovoltaic Specialists Conference, pp. 710–714. IEEE Press, New York (1985)

46. Bank, R.E., Rose, D.J., Fichtner, W.: IEEE Trans. Electron Devices **30**, 1031 (1983)

47. Müller, S., Kells, K., Fichtner, W.: IEEE Trans. Comput.-Aided Des. Integr. Circuits Syst. **11**, 855 (1992)

48. Heiser, G., Pommerell, C., Weis, J., Fichtner, W.: IEEE Trans. Comput.-Aided Des. Integr. Circuits Syst. **10**, 1218 (1991)

49. Aberle, A.G., Heiser, G., Green, M.A.: Sol. Energy Mater. Sol. Cells **34**, 149 (1994)

50. Heiser, G., Aberle, A.G., Wenham, S.R., Green, M.A.: Microelectron. J. **26**(2/3), 273 (1995)

51. Aberle, A.G., Altermatt, P.P., Heiser, G., Robinson, S.J., Wang, A., Zhao, J., Krumbein, U., Green, M.A.: J. Appl. Phys. **77**, 3491 (1995)

52. Zhao, J., Wang, A., Altermatt, P., Green, M.A.: Appl. Phys. Lett. **66**, 3636 (1995)

53. Altermatt, P.P., Heiser, G., Aberle, A.G., Wang, A., Zhao, J., Robinson, S.J., Bowden, S., Green, M.A.: Prog. Photovolt. **4**, 399 (1996)

54. Glunz, S.W., Schumacher, J., Warta, W., Knobloch, J., Wettling, W.: Prog. Photovolt. **4**, 415 (1996)

55. Schumacher, J.O., Hebling, C., Warta, W.: In: Proceedings of the 14th European Photovoltaic Solar Energy Conference, pp. 1467–1471. H.S. Stephens and Associates, Bedford (1997)

56. Granek, F., Hermle, M., Huljic, D.M., Schultz-Wittmann, O., Glunz, S.W.: Prog. Photovolt. **17**, 47 (2009)

57. Kluska, S., Granek, F., Ruediger, M., Hermle, M., Glunz, S.W.: Sol. Energy Mater. Sol. Cells **94**, 568 (2010)

58. Schön, J., Warta, W.: In: Proceedings of the 23rd European Photovoltaic Solar Energy Conference, pp. 1851–1854. WIP-Renewable Energies, Munich (2008)

59. Zechner, C., Fath, P., Willeke, G., Bucher, E.: In: Proceedings of the 14th European Photovoltaic Solar Energy Conference, pp. 69–72. H.S. Stephens and Associates, Bedford (1997)

60. Hahn, G., Zechner, C., Rinio, M., Fath, P., Willeke, G., Bucher, E.: J. Appl. Phys. **86**, 7179 (1999)

61. Aberle, A.G., Kuhlmann, B., Meyer, R., Hübner, A., Hampe, C., Hezel, R.: Prog. Photovolt. **4**, 193 (1996)

62. Kuhlmann, B., Aberle, A.G., Hezel, R.: IEEE Trans. Electron Devices **47**, 2167 (2000)

63. Altermatt, P.P., Dreissigacker, S., Yang, Y., Sprodowski, C., Dezhdar, T., Koc, S., Veith, B., Herrman, S., Bock, R., Bothe, K., Schmidt, J., Brendel, R.: In: Proceedings of the 24th European Photovoltaic Solar Energy Conference, pp. 901–906. WIP-Renewable Energies, Munich (2009)

64. Nijs, J., Demesmaeker, E., Szlufcik, J., Poortmans, J., Frisson, L., De Clercq, K., Ghannam, M.: In: Proceedings of the 1st World Conference on Photovoltaic Energy Conversion, pp. 1242–1249. IEEE Press, New York (1994)

65. Peters, S., Leihkauf, R., Wagemann, H.G., Boit, C.: In: Proceedings of the 19th European Photovoltaic Solar Energy Conference, pp. 690–693. WIP-Renewable Energies, Munich (2004)

66. Franklin, E., Blakers, A.: In: Proceedings of the 19th European Photovoltaic Solar Energy Conference, pp. 1149–1152. WIP-Renewable Energies, Munich (2004)

67. Nakamura, K., Isaka, T., Funakoshi, Y., Tonomura, Y., Machida, T., Okamoto, K.: In: Proceedings of the 20th European Photovoltaic Solar Energy Conference, pp. 789–792. WIP-Renewable Energies, Munich (2005)

68. Lu, M., Bowden, S., Das, U., Birkmir, R.: In: Proceedings of the 22nd European Photovoltaic Solar Energy Conference, pp. 924–927. WIP-Renewable Energies, Munich (2007)

69. Ahn, C., Drew, K., Cole, A., Heasman, K.C., Brown, L., Cowern, N.E.B.: In: Proceedings of the 25th European Photovoltaic Solar Energy Conference, pp. 2548–2553. WIP-Renewable Energies, Munich (2010)

70. Aleman, M., Rosseel, E., van Wichelen, K., Pawlak, B.J., Janssens, T., Dross, F., Posthuma, N.E., Poortmans, J.: In: Proceedings of the 35th IEEE Photovoltaic Specialists Conference, pp. 296–299. IEEE Press, New York (2010)

71. Heiser, G., Altermatt, P.P., Williams, A., Sproul, A., Green, M.A.: In: Proceedings of the 13th European Photovoltaic Solar Energy Conference, pp. 447–450. H.S. Stephens and Associates, Bedford (1995)

72. Altermatt, P.P., Heiser, G.: J. Appl. Phys. **91**, 4271 (2002)

73. Altermatt, P.P., Heiser, G.: J. Appl. Phys. **92**, 2561 (2002)

74. Ulzhöfer, C., Altermatt, P.P., Harder, N.P., Brendel, R.: J. Appl. Phys. **107**, 104509 (2010)

75. Kelzenberg, M.D., Turner-Evans, D.B., Kayes, B.M., Filler, M.A., Putnam, M.C., Lewis, N.S., Atwater, H.A.: In: Proceedings of the 33rd IEEE Photovoltaic Specialists Conference, pp. 39–44. IEEE Press, New York (2008)

76. Kelzenberg, M.D., Putnam, M.C., Turner-Evans, D.B., Lewis, N.S., Atwater, H.A.: In: Proceedings of the 34th IEEE Photovoltaic Specialists Conference, pp. 112–117. IEEE Press, New York (2009)

77. Conti, P., Tomizawa, M., Yoshii, A.: Int. J. Numer. Methods Eng. **37**, 3211 (1994)

78. Altermatt, P.P., Heiser, G., Green, M.A.: Prog. Photovolt. **4**, 355 (1996)

79. Wasserrab, T.: Z. Naturforsch. A **32**, 746 (1977)

80. Sproul, A.B., Green, M.A.: In: Proceedings of the 21st IEEE Photovoltaic Specialists Conference, pp. 380–385. IEEE Press, New York (1990)

81. Sproul, A.B., Green, M.A.: J. Appl. Phys. **70**, 846 (1991)

82. Misiakos, K., Tsamakis, D.: J. Appl. Phys. **74**, 3293 (1993)

83. Altermatt, P.P., Schenk, A., Geelhaar, F., Heiser, G.: J. Appl. Phys. **93**, 1598 (2003)

84. Schenk, A.: J. Appl. Phys. **84**, 3684 (1998)

85. del Alamo, J.A., Swanson, R.M.: Solid-State Electron. **30**, 1127 (1987)

86. Klaassen, D.B.M., Slotboom, J.W., de Graaff, H.C.: Solid-State Electron. **35**, 125 (1992)

87. Glunz, S.W., Dicker, J., Altermatt, P.P.: In: Proceedings of the 17th EU Photovoltaic Energy Conference, Munich, Germany, pp. 1391–1395. WIP/ETA, Munich/Florence (2001)

88. Green, M.A.: J. Appl. Phys. **67**, 2944 (1990)

89. Pässler, R.: Phys. Rev. B **66**, 085201 (2002)

90. Pässler, R.: Phys. Status Solidi B **216**, 975 (1999)

91. Pässler, R.: Phys. Status Solidi B **236**, 710–728 (2003)

92. Lundstrom, M.S., Schwartz, R.J., Gray, J.L.: Solid-State Electron. **24**, 195 (1981)

93. Kroemer, H.: RCA Rev. **28**, 332 (1957)
94. Kane, D.E., Swanson, R.M.: In: Proceedings of the 18th IEEE Photovoltaic Specialists Conference, pp. 578–583. IEEE Press, New York (1985)
95. Sinton, R.A., Cuevas, A.: Appl. Phys. Lett. **69**, 2510 (1996)
96. Sinton, R., Cuevas, A., Stuckings, M.: In: Proceedings of the 25th IEEE Photovoltaic Specialists Conference, pp. 457–460. IEEE Press, New York (1996)
97. Kerr, M.J., Cuevas, A., Sinton, R.A.: J. Appl. Phys. **91**, 399 (2002)
98. Cuevas, A., Sinton, R.A.: Prog. Photovolt. **5**, 79 (1997)
99. Altermatt, P.P., Schumacher, J.O., Cuevas, A., Kerr, M.J., Glunz, S.W., King, R.R., Heiser, G., Schenk, A.: J. Appl. Phys. **92**, 3187 (2002)
100. Altermatt, P.P., Plagwitz, H., Bock, R., Schmidt, J., Brendel, R., Kerr, M.J., Cuevas, A.: In: Proceedings of the 21st European Photovoltaic Solar Energy Conference, pp. 647–650. WIP-Renewable Energies, Munich (2006)
101. Hoex, B., Schmidt, J., Bock, R., Altermatt, P.P., van de Sanden, M.C.M., Kessels, W.M.M.: Appl. Phys. Lett. **91**, 112107 (2007)
102. Blakemore, J.S.: Solid-State Electron. **25**, 1067 (1982)
103. Cohen, M.H., Chou, M.Y., Ecoonomou, E.N., Jahn, S., Soukoulis, C.M.: IBM J. Res. Dev. **32**, 82 (1988)
104. John, S., Chou, M.Y., Cohen, M.H., Soukoulis, C.M.: Phys. Rev. B **37**, 6963 (1988)
105. Serre, J., Ghazali, A.: Phys. Rev. B **28**, 4704 (1983)
106. Ghazali, A., Serre, J.: Solid-State Electron. **28**, 145 (1985)
107. Solmi, S., Parisini, A., Angelucci, R., Armigliato, A., Nobili, D., Moro, L.: Phys. Rev. B **53**, 7836 (1996)
108. Klaassen, D.B.M.: Solid-State Electron. **35**, 953 (1992)
109. Klaassen, D.B.M.: Solid-State Electron. **35**, 961 (1992)
110. Rougieux, F.E., Macdonald, D., Cuevas, A., Ruffell, S., Schmidt, J., Lim, B., Knights, A.P.: J. Appl. Phys. **108**, 013706 (2010)
111. Geilker, J., Kwapil, W., Reis, I., Rein, S.: In: Proceedings of the 25th European Photovoltaic Solar Energy Conference, pp. 1322–1327. WIP-Renewable Energies, Munich (2010)
112. Schindler, F., Geilker, J., Kwapil, W., Giesecke, J., Schubert, M., Warta, W.: In: Proceedings of the 25th European Photovoltaic Solar Energy Conference, pp. 2364–2368. WIP-Renewable Energies, Munich (2010)
113. Lim, B., Wolf, M., Schmidt, J.: Phys. Status Solidi C **8**, 835 (2011)
114. Kane, D.E., Swanson, R.M.: In: Proceedings of the 20th IEEE Photovoltaic Specialists Conference, pp. 512–517. IEEE Press, New York (1988)
115. Kane, D.E., Sinton, R.A., Gan, J.Y., Swanson, R.M.: In: Proceedings of the 21st IEEE Photovoltaic Specialists Conference, pp. 437–441. IEEE Press, New York (1990)
116. Kane, D.E., Swanson, R.M.: J. Appl. Phys. **73**, 1193 (1993)
117. Green, M.A.: Silicon Solar Cells: Advanced Principles and Practice. Photovoltaics Special Research Centre, University of New South Wale, Sydney (1995). ISBN 0-7334-0994-6
118. Corkish, R., Chan, D.S.P., Green, M.A.: J. Appl. Phys. **79**, 195 (1996)
119. Karazhanov, S.Z.: J. Appl. Phys. **82**, 5807 (1997)
120. Karazhanov, S.Z.: Sol. Energy Mater. Sol. Cells **63**, 149 (2000)
121. Combescot, M.: Phys. Status Solidi B **86**, 349 (1978)
122. Geelhaar, F.: Coulomb Correlation Effects in Silicon Devices. Series in Microelectronics, vol. 147. Hartung-Gorre, Konstanz (2004)
123. Macdonald, D., Cuevas, A.: Phys. Rev. B **67**, 075203 (2003)
124. Shockley, W., Read, W.: Phys. Rev. **87**, 835 (1952)
125. Hall, R.: Phys. Rev. **87**, 387 (1952)
126. Sah, C.T., Shockley, W.: Phys. Rev. **109**, 1103 (1958)
127. Willemen, J.A.: Ph.D. thesis, Technical University Delft, The Netherlands (1998)
128. Queisser, H.J.: Solid-State Electron. **5**, 1 (1962)
129. Breitenstein, O., Langenkamp, M., Lang, O., Schirrmacher, A.: Sol. Energy Mater. Sol. Cells **65**, 55 (2001)
130. Kendall, D.: Presented at the Conference for Physics and Application of Lithium Diffused Silicon, NASA Space Flight Center, Goddard, FL (1969)
131. Schmidt, J., Aberle, A.G.: J. Appl. Phys. **81**, 6186 (1997)
132. Altermatt, P.P., Schmidt, J., Heiser, G., Aberle, A.G.: J. Appl. Phys. **82**, 4938 (1997)
133. Brendel, R.: Appl. Phys. A **60**, 523 (1995)
134. Aberle, A.G., Schmidt, J., Brendel, R.: J. Appl. Phys. **79**, 1491 (1996)
135. Schmidt, J.: IEEE Trans. Electron Devices **46**, 2018 (1999)
136. Schuurmans, F.M., Schönecker, A., Burgers, A.R., Sinke, W.C.: Appl. Phys. Lett. **71**, 1795 (1997)
137. Robinson, S.J., Aberle, A.G., Green, M.A.: IEEE Trans. Electron Devices **41**, 1556 (1994)
138. Schmidt, J., Cuevas, A., Rein, S., Glunz, S.W.: Prog. Photovolt. **9**, 249 (2001)
139. Schmidt, J., Cuevas, A.: J. Appl. Phys. **86**, 3175 (1999)
140. Rein, S., Glunz, S.W.: Appl. Phys. Lett. **82**, 1054 (2003)
141. Bothe, K., Sinton, R., Schmidt, J.: Prog. Photovolt. **13**, 287 (2005)
142. Fischer, H., Pschunder, W.: In: Proceedings of the 10th IEEE Photovoltaic Specialists Conference, pp. 404–411. IEEE Press, New York (1973)
143. Schmidt, J.: Appl. Phys. Lett. **82**, 2178 (2003)
144. Schmidt, J., Thiemann, N., Bock, R., Brendel, R.: J. Appl. Phys. **106**, 093707 (2009)
145. Bock, R., Altermatt, P.P., Schmidt, J., Brendel, R.: Semicond. Sci. Technol. **25**, 105007 (2010)
146. Rüdiger, M., Rauer, M., Schmiga, C., Hermle, M.: Effect of incomplete ionization for the description of highly aluminum-doped silicon (to be published)
147. Steingrube, S., Steingrube, D.S., Brendel, R., Altermatt, P.P.: Phys. Status Solidi C **7**, 276 (2010)
148. Rein, S., Rehrl, T., Warta, W., Glunz, S.W.: J. Appl. Phys. **91**, 2059 (2002)
149. McIntosh, K.R., Paudyal, B.B., Macdonald, D.H.: J. Appl. Phys. **104**, 084503 (2008)
150. Steingrube, S., Altermatt, P.P., Steingrube, D.S., Schmidt, J., Brendel, R.: J. Appl. Phys. **108**, 014506 (2010)
151. Steingrube, S., Altermatt, P., Zielke, D., Werner, F., Schmidt, J., Brendel, R.: In: Proceedings of the 25th European Photovoltaic Solar Energy Conference, pp. 1748–1754. WIP-Renewable Energies, Munich (2010)
152. Cuevas, A., Macdonald, D.: Sol. Energy **76**, 255 (2004)
153. Dziewior, J., Schmid, W.: Appl. Phys. Lett. **31**, 346 (1977)
154. Hangleiter, A., Häcker, R.: Phys. Rev. Lett. **65**, 215 (1990)
155. Häcker, R., Hangleiter, A.: J. Appl. Phys. **75**, 7570 (1994)
156. Sinton, R., Swanson, R.: IEEE Trans. Electron Devices **34**, 1380 (1987)
157. Glunz, S.W., Biro, D., Rein, S., Warta, W.: J. Appl. Phys. **86**, 683 (1999)
158. Schmidt, J., Kerr, M., Altermatt, P.P.: J. Appl. Phys. **88**, 1494 (2000)
159. Kerr, M.J., Cuevas, A.: J. Appl. Phys. **91**, 2473 (2002)
160. Reichel, C., Granek, F., Benik, J., Schultz-Wittmann, O., Glunz, S.W.: In: Proceedings of the 23rd European Photovoltaic Solar Energy Conference, pp. 1664–1669. WIP-Renewable Energies, Munich (2008)
161. Yablonovitch, E., Gmitter, T.: Solid-State Electron. **35**, 261 (1992)
162. Altermatt, P.P., Geelhaar, F., Trupke, T., Dai, X., Neisser, A., Daub, E.: Appl. Phys. Lett. **88**, 261901 (2006)

163. Altermatt, P.P., Geelhaar, F., Trupke, T., Day, X., Neisser, A., Daub, E.: In: Proceedings of the 5th International Conference on Numerical Simulation of Optoelectronic Devices (NUSOD05), pp. 47–48. IEEE Press, New York (2005)

164. Trupke, T., Green, M.A., Würfel, P., Altermatt, P.P., Wang, A., Zhao, J., Corkish, R.: J. Appl. Phys. **94**, 4930 (2003)

165. Trupke, T., Daub, E., Würfel, P.: Sol. Energy Mater. Sol. Cells **53**, 103 (1998)

166. Daub, E., Würfel, P.: Phys. Rev. Lett. **74**, 1020 (1995)

167. Daub, E., Würfel, P.: J. Appl. Phys. **80**, 5325 (1996)

168. Smith, A.W., Rohatgi, A., Neel, S.C.: In: Proceedings of the 21st IEEE Photovoltaic Specialists Conference, pp. 426–431. IEEE Press, New York (1990)

169. Brendel, R.: In: Proceedings of the 12th European Photovoltaic Solar Energy Conference, pp. 1339–1342. H.S. Stephens and Associates, Bedford (1994)

170. Schumacher, J., Sterk, S., Wagner, B., Warta, W.: In: Proceedings of the 13th European Photovoltaic Solar Energy Conference, pp. 96–99. H.S. Stephens and Associates, Bedford (1995)

171. Zechner, C., Fath, P., Willeke, G., Bucher, E.: Sol. Energy Mater. Sol. Cells **51**, 255 (1998)

172. Cotter, J.E.: In: Proceedings of the 31st IEEE Photovoltaic Specialists Conference, pp. 1165–1168. IEEE Press, New York (2005)

173. Holst, H., Altermatt, P.P., Brendel, R.: In: Proceedings of the 25th European Photovoltaic Solar Energy Conference, pp. 2150–2153. WIP-Renewable Energies, Munich (2010)

174. Blakers, A.W.: J. Appl. Phys. **71**, 5237 (1992)

175. Stuckings, M., Blakers, A.: Sol. Energy Mater. Sol. Cells **59**, 233 (1999)

176. Woehl, R., Hörteis, M., Glunz, S.W.: In: Proceedings of the 23rd European Photovoltaic Solar Energy Conference, pp. 1377–1382. WIP-Renewable Energies, Munich (2008)

177. Yang, Y., Altermatt, P.P.: In: Proceedings of the European COMSOL Conference, p. 5259. COMSOL, Hannover (2008)

178. Clugston, D.A., Basore, P.A.: Prog. Photovolt. **5**, 229 (1997)

179. Isenberg, J., Warta, W.: J. Appl. Phys. **84**, 2265 (2004)

180. Macleod, H.A.: Thin-Film Optical Filters, 3rd edn. Institute of Physics Publishing, Philadelphia (2001)

181. Gueymard, C.A., Myers, D., Emery, K.: Sol. Energy **73**, 443 (2002)

182. Gueymard, C.: Sol. Energy **71**, 325 (2001)

183. Green, M.A.: Sol. Energy Mater. Sol. Cells **92**, 1305 (2008)

184. Shiles, E., Sasaki, T., Inokuti, M., Smith, D.Y.: Phys. Rev. B **22**, 1612 (1980)

185. Palik, E.D.: Handbook of Optical Constants of Solids. Academic Press, San Diego (1985)